WRAP-AROUND SENSORS FOR ELECTRICAL DETECTION OF PARTICLES IN MICROFLUIDIC CHANNELS

Ozgun Civelekoglu,[a] Ruxiu Liu,[a] Norh Asmare,[a] A K M Arifuzzman,[a] and A. Fatih Sarioglu [abc]

[a] School of Electrical and Computer Engineering, Georgia Institute of Technology, Atlanta, GA, United States
[b] Institute for Electronics and Nanotechnology, Georgia Institute of Technology, Atlanta, GA, United States
[c] Parker H. Petit Institute for Bioengineering and Bioscience, Georgia Institute of Technology, Atlanta, GA, United States

ABSTRACT

Microfluidic devices with integrated electrical sensors have been widely employed in the detection and characterization of particles suspended in liquids. Conventionally, electrical sensors in microfluidic devices are composed of electrodes all patterned on the same surface in a coplanar arrangement. While simplifying the fabrication of electrical sensors within microfluidic channels considerably, the use of coplanar electrodes leads to non-uniform electric fields within the channel and complicates scaling of electrical sensor networks by constraining the routing of different traces within the same plane. The alternative of integrating counter-facing parallel electrodes into microfluidic channels to alleviate those limitations requires a complex fabrication process. In this work, we present a robust and straightforward approach to creating 3D electrical sensors in microfluidic devices fabricated using soft lithography. By placing a blanket electrode on the microfluidic channel walls, our electrical sensor wraps around the flow channel and (i) provide higher sensitivity than their coplanar counterparts, (ii) extend the sensing volume beyond the vicinity of a surface and (iii) simplify the creation of electrical sensor networks with complex geometries by relaxing the routing constraints on traces. Practical implementation of 3D electrical sensors in microfluidic channels offers the potential to enhance the utility of electrical sensing without impacting the frugality of fluidic components in designing integrated microfluidic systems as quantitative platforms.

Keywords: Microfluidic impedance spectroscopy; 3D electrodes; microfabrication; soft lithography

1. INTRODUCTION

Detecting, counting, and characterizing micro-/nano-particles in liquids rapidly and reliably is a process that is invaluable in various biomedical [1-3], environmental [4-6], and industrial applications [7, 8]. Analysis of small particles suspended in liquids through electrical sensors [9-12], provides an easy and robust detection scheme with less hardware overhead compared to optical techniques such as microscopy and dynamic light scattering [13]. In a typical electrical sensor, two electrodes separated by an aperture are placed under a potential difference, and the electrical current between those electrodes is continuously monitored to sense impedance variations. Due to differences between the electrical properties of the particles and the surrounding electrolyte, particles passing through the aperture in between electrodes produce momentary changes in the impedance and hence the electrical current. An analysis of the electrical current therefore enables enumeration, sizing, and impedance spectroscopy of particles. This simple and robust mechanism forms the basis of Coulter counters, which are widely used in research and clinical laboratories [14].

Integration of electrical sensors into microfluidic channels has long been pursued to achieve a quantitative analysis of particles in a well-defined microenvironment with high sensitivity afforded by a precisely manufactured aperture [15]. In fact, such integrated systems in micro-scale have been demonstrated to be instrumental in detecting chemical/biological particles such as proteins [16], interleukins [17], cells [18-23], DNA/RNA molecules [24], bacteria [25, 26], extracellular vesicles [27, 28]. Conventionally, electrical sensors are readily implemented in microfluidic channels in the form of two coplanar electrodes on the floor of the channels [29, 30]. Under a potential difference, an electric field is established between the electrodes, and the volume between the electrodes acts as the sensor's aperture. This coplanar configuration has long been the design of choice as it can be manufactured with a simple fabrication process that is compatible with soft lithography [31]. As attractive as it may be from a fabrication point of view, constraining electrodes onto a single plane however not only leads to non-uniform electric fields and reduced sensor performance [32-34], but also complicates the scaling of the sensors to form a network due to restrictive routing of opposite polarity traces within the same plane [35-37].

In contrast, an electrical sensor composed of electrodes placed on different planes distribute electric field across the channel cross-section leading to larger detection volume and provide an extra layer for electrode routing for complex sensor network layouts. As such, counter-facing electrodes on parallel surfaces have been theoretically investigated as electrical sensors using analytical [38] and numerical [39-41] analyses. Sensors based on counter-facing electrodes have also been manufactured in microfluidic channels using a variety of microfabrication methods, including surface functionalization at the atomic level [42], etching of a polymer film to reveal underlying metal film [43], peel-off [44, 45], and multi-stage photolithography [46] and were shown to be functional in micro- [47, 48] and nano- [45] biosensors for detection of particles [48-50], bacteria [51] and DNA [52]. While effective, the experimental realization of these multi-planar electrical sensors typically relied on fabrication processes that require photolithography on multiple substrates as well as precise alignment during bonding, making the whole process significantly more complex than the integration of planar electrical sensors.

In this paper, we introduce an electrical sensor formed by electrodes wrapping around the

microfluidic channel and a robust and straightforward fabrication technique to create these sensors in microfluidic devices fabricated using soft lithography. In our wrap-around sensor (Figure 1a), we create a blanket electrode that is deposited selectively onto the walls of the microfluidic channel, leaving the substrate to be patterned only for the counter electrode. This electrode arrangement allows the electric field to permeate across the whole channel cross-section, leading to higher detection sensitivity. In addition, the design and scaling of sensor architectures are simplified as the counter electrodes are now routed on two different planes without constraints.

2. MATERIALS AND METHODS

2.1. Computational modeling parameters

The electrical properties of the cell were set to a conductivity of 0.5 S/m and a permittivity of 60 [53]. A 100 nm-thick cell membrane was approximated by the contact impedance boundary condition assuming the membrane conductivity and the membrane's relative permittivity to be 10^{-8} S/m and 11, respectively. The medium (the material of the rectangular block representing the microfluidic channel) was modeled as a dilute solution of PBS with the conductivity of 1.4 S/m and the relative permittivity of 80. The excitation electrodes were set to carry an electric potential of 1 V, and the sensing electrodes were set as the electrical ground. An insulating boundary condition was applied to all other boundaries. The data shown in Figure 3b and 3c were acquired by simulating a cell with a diameter of 7 μm in a channel that is 30 μm-wide and 65 μm-tall, and a cell with a diameter of 5 μm in a 30 μm-wide, 15 μm-tall channel, respectively. The width of micropatterned electrodes were set to be 10 μm, which falls in the range of reported electrode sizes reported for cell detection [16, 19-21].

2.2. Cell culture

We tested our device using human MDA-MB-231 breast cancer cells suspended in phosphate buffered saline (PBS) as the biological sample. The cells were obtained from ATCC and cultured in DMEM media supplemented with 10% fetal bovine serum (FBS) and maintained under 5% CO2 atmosphere at 37 C until 80% confluence was reached. The cells were then detached using a 0.25% trypsin solution, pelleted in a centrifuge, resuspended in 1X PBS, and mixed by gentle pipetting to dissociate the cell aggregates.

2.3. Electrical signal acquisition.

Our experimental setup includes a syringe pump for driving the biological sample into our device, the electrical hardware for data acquisition, and the custom software for data analysis. The cell suspension was collected in a 1mL syringe and driven into the device at a flow rate of 100 μL/h using a syringe pump (Harvard Apparatus). The output signal of the lock-in amplifier (HF2LI, Zurich Instruments) was connected to the blanket electrode via the auxiliary connection port, filled with electrically conductive epoxy (8331, MG Chemicals). The electrical connections to the planar electrodes on the glass substrate were made by soldering copper jumper wires to connection pads. A 500 kHz sine wave with a 100-mV amplitude was applied to the blanket electrode layer to excite the system. The currents from both sensing electrodes were measured using two trans-impedance amplifiers (HF2TA, Zurich Instruments), subtracted from each other using a differential amplifier, and measured using a lock-in amplifier. The signal output was then transmitted to the computer through a data acquisition board (PCIe-6361,

National Instruments) at a sample rate of 50 kHz, the recording and the analysis of the signals were done by a custom MATLAB program.

2.4. Signal processing

The device signals were sampled into a computer at 500 kHz, low-pass filtered with a cut-off frequency of 2 kHz and were processed using MATLAB. Peaks in the sampled signal were identified as local extremum points that exceeded a threshold set above the background noise level. For two-electrode sensors, the amplitude and signal duration were recorded for each peak and scored as a cell. For differential signals from multi-electrode sensors, the peak amplitude was determined from the average amplitude of the corresponding positive and negative peaks, and the signal duration was determined as the time from the start of the rising edge of the first peak and the end of the falling edge of the last peak.

2.5. Calibration of cell size

As the signal amplitude from impedance-based electrical counters has a linear relationship with the cell's volume [10], we calibrated our signal amplitude with microbeads. We specifically used polystyrene beads (Cat No: 17136-5, Polysciences) that were 10 μm in diameter for their similar size to cells and their exceptional uniformity. After processing more than 5,000 beads with our system, we set the mean signal amplitude to represent the volume of a cell with a 10-micron diameter.

3. RESULTS

3.1. Sensor Design

Our wrap-around sensor is composed of a blanket electrode covering the inner walls of a microfluidic channel coupled with a conventional micromachined electrode on the floor of the microfluidic channel (Figure 1a). When taken as a pair, these two electrodes lined along the inner walls of a microfluidic channel wraps around the whole cross-section, except at the intentionally left gaps to electrically isolate them. From a geometrical perspective, our electrode layout can be considered analogous to the 3-D gate electrodes used in the construction of fin field-effect transistors (FinFETs) [54, 55] to improve the control of channel electrical conductivity through an electric field.

Similar to FinFETs, our goal in creating wrap-around sensors is to increase the extent of the electric field across the whole microfluidic channel cross-section but for detection and potentially for manipulating suspended micro- and nanoparticles. Compared to conventional sensor designs based on coplanar electrodes, our electrode layout allows electric field lines to form between the channel floor and each of the inner surfaces of the microfluidic channel (Figure 1b). In this way, the conductive walls of the microfluidic channel effectively spread the field beyond a single surface and result in an increase in the electrically active volume.

In our design, the blanket electrode was made to cover the walls of the microfluidic channels indiscriminately, with the wrap-around sensor being defined at device locations where the blanket electrode counter-faced with a surface micromachined electrode on the substrate (Figure 1c). Therefore, from a design perspective, the blanket electrode acted similar to a ground plane in a printed circuit board, creating a low impedance "highway" for the electrical potential difference to be delivered wherever the microfluidic are present in our device with

minimal resistive losses (Figure 1d). Indeed, metallizing the ceiling of a microfluidic channel was previously shown to increase the conductance of the power-carrying electrode leading to smaller fluctuations in electrical potential [45]. To electrically interface with the blanket electrode, a section of microfluidic channel, where there were no surface counter electrodes, was filled with a conductive epoxy and a copper wire merged with the epoxy provided the connection to the external circuitry through a punched-out port in the polymer.

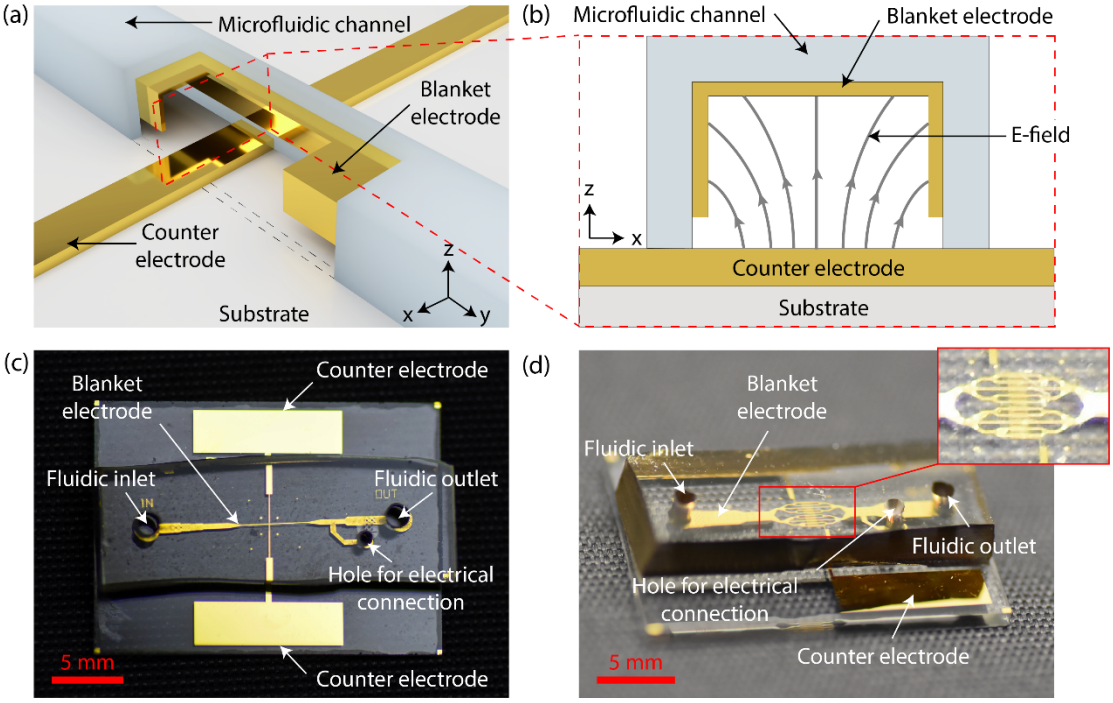

Figure 1. The design of the wrap-around sensor. (a) A computer drawing illustrating the components of the wrap-around sensor. The inner surfaces of a microfluidic channel are coated with a metal film as a medium for carrying the electrical excitation along with the fluids in the channel. (b) The inset shows a schematic showing the cross-sectional view of a microfluidic channel equipped with the wrap-around sensor and the electric field lines between the blanket electrode and the counter electrode on the floor of the channel. (c) A photo showing the top-view of a manufactured microfluidic device integrated with a wrap-around sensor. The optically transparent PDMS-based microfluidic channel is seen as yellow from the inlet to the outlet as it is coated with the blanket electrode. The counter electrode on the glass slide is a single electrode trace that crosses the microfluidic channel. (d) A photo showing a microfluidic device integrated with multiple wrap-around sensors for the detection of particles flowing through multiple microfluidic channels. The inset shows a close-up image of the layout.

3.2. Microfabrication process

The wrap-around sensors in microfluidic channels were fabricated in two steps: First, a blanket electrode was placed on the inner walls of the microfluidic channel. Then, planar surface electrodes were micromachined on a substrate. The two electrodes were coupled to complete the sensor fabrication.

The fabrication process (Figure 2a) started by creating microfluidic channels with soft

lithography. To fabricate the mold, an SU-8 negative photoresist film was first uniformly spun on a 4-inch silicon wafer, and then the photoresist was patterned with photolithography using a maskless aligner (MLA150, Heidelberg). Polydimethylsiloxane (PDMS) polymer and cross-linker were then mixed at a 10:1 ratio, poured on the mold, degassed, and baked at 65 °C for at least 4 hours. Once cured, the PDMS layer was peeled from the mold and diced into small pieces. The fluidic ports (i.e., inlet and outlet), as well as additional ports that will be used for electrical connections were all created at once with a biopsy punch.

Next, we created a blanket electrode on the inner walls of the fabricated microfluidic channel. To form the blanket electrode, we developed a process to selectively deposit a metal film on the flexible PDMS substrate that was previously patterned with the microfluidic features. As part of this process, the PDMS substrate was first coated with a 100 nm-thick gold film via sputtering. Because this deposition process resulted in a conformal coating of the whole PDMS surface, the gold film needed to be selectively etched from the bonding surface to prevent a short circuit with the counter electrode. To remove the gold film on the bonding surface of the PDMS substrate, we used adhesive tape, which exclusively removed the gold that came in contact with the adhesive polymer on the tape. Furthermore, because the adhesive film extended slightly into the microfluidic channels on PDMS when pressed against the tape under a mild force, parts of the sidewalls in the vicinity of the bonding surface were also cleared of the gold, as confirmed with scanning electron micrographs (Figure 2b). Taken together, this tape-assisted etching process selectively removed the gold film on the surface and its vicinity, electrically insulating it from a counter-electrode. It should also be noted that removing deposited gold film via stiction to an adhesive tape was only possible as purposedly no adhesion-promoting layer, such as chromium or titanium, was used before gold deposition in the fabrication process.

Next, we fabricated the counter electrodes conventionally on a planar surface through a lift-off process. Briefly, a 1.2 μm-thick negative photoresist (NR9-1500PY) was first spun on a glass slide and patterned with conventional photolithography using a maskless aligner (MLA150, Heidelberg). After the development of the exposed photoresist, a 20-nm Cr film followed by 80-nm Au film was deposited on the glass substrate via e-beam evaporation. The lift-off process was completed by etching the sacrificial photoresist film in acetone under mild sonication.

Finally, we coupled the blanket electrode placed on the walls of the microfluidic channel with surface micromachined counter electrodes to complete our sensor. To bond the PDMS and glass substrates, both surfaces were first activated under oxygen plasma, aligned under a microscope and permanently bonded on a hot plate at 65°C. To electrically interface with the blanket electrode, a copper wire was inserted into the punched-out auxiliary port and the port was filled with conductive epoxy (MG Chemicals 8331), which ensured a steady electrical and a leak-free operation.

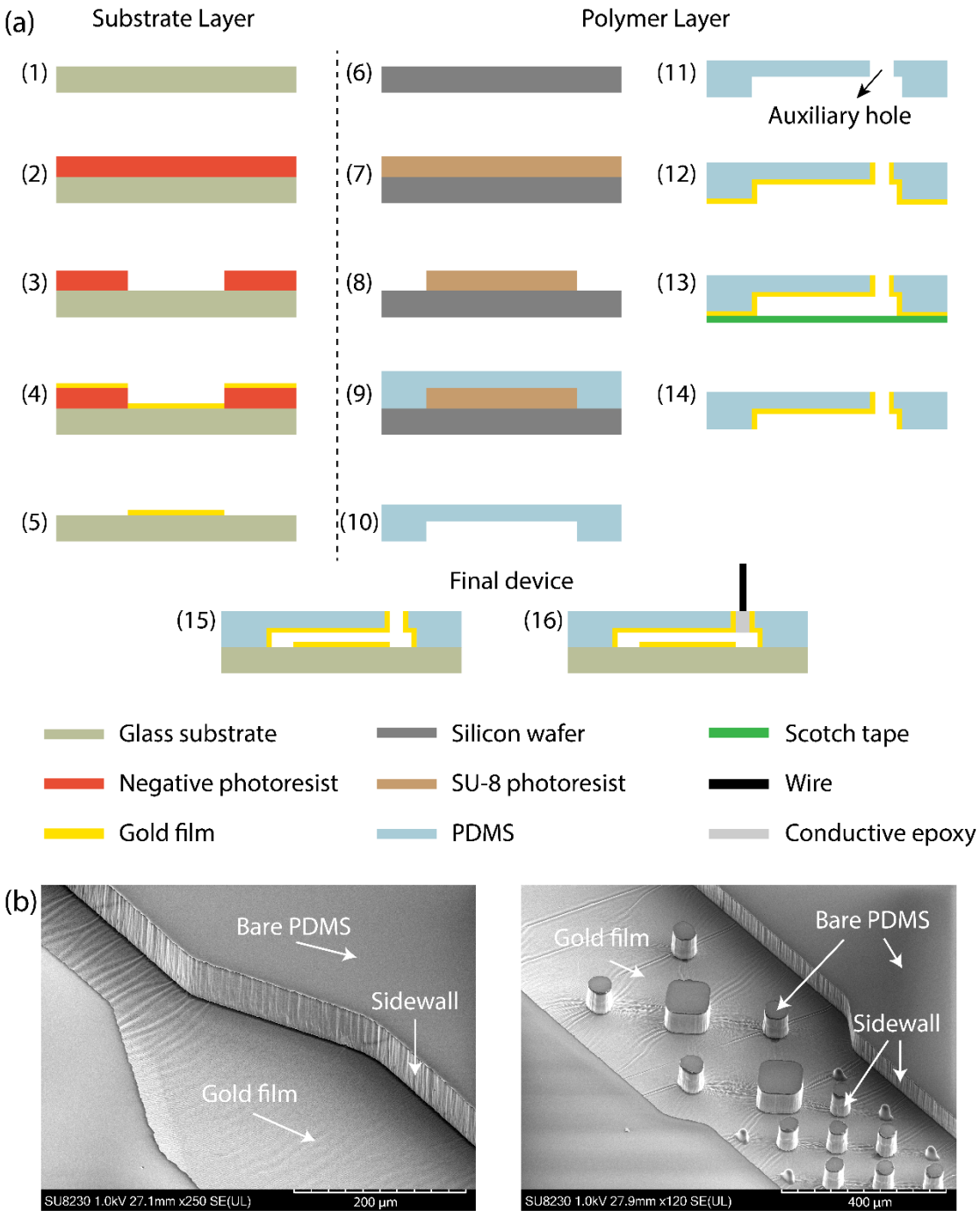

Figure 2. Microfabrication process. (a) A schematic showing the cross-sectional images corresponding to individual steps of the developed microfabrication process. (b) Scanning electron micrographs of gold-coated microfluidic channels molded in PDMS using soft lithography. The gold film coatings on the sidewalls and channel ceiling can be deduced from the wrinkles visible in the sputtered film.

3.3. Computational Analysis of Sensor Operation

To analyze the operation of the wrap-around sensor, we first investigated the electrical field distribution within a microfluidic channel when integrated with the sensor (Figure 3a). We created a computational model of the sensor electrode configuration and simulated the electrical field with finite element analysis using a commercially available software (COMSOL Multiphysics v5.4). To simulate the interaction of the sensor with a particle, we placed a circular object in the channel cross-section with electrical parameters set based on the representative electrical properties of a biological cell available in the literature (Materials and Methods). In addition, the channel was assumed to be filled with phosphate buffered saline (PBS) as the electrolyte. The simulated electric field intensity within the wrap-around sensor was found to be nonuniform in the channel cross-section due to the size difference between the blanket and the counter electrode. Specifically, the fringing electric field at the edges of the counter electrode was found to be directed towards the channel sidewalls horizontally. Towards the center of the counter electrode, the electric field steered towards the ceiling of the microfluidic channel, eventually converging to a vertical profile. Taken together, these simulations demonstrated a sensor-induced electric field profile that is dispersed across the microfluidic channel cross-section and demonstrated its potential to detect particles throughout the sensing volume.

To place the simulated electric field distribution of the wrap-around sensor into perspective, we compared it with the simulated electric field distributions due to conventional (i.e., coplanar and parallel) configurations of sensing electrodes in microfluidic channels (Figure 3). When compared to the coplanar electrodes, the wrap-around sensor configuration extended the electric field lines further towards the ceiling of the microfluidic channel. The presence of the blanket electrode over the ceiling was found to increase the field intensity vertically while still producing a non-uniform field distribution. In comparison, the parallel electrode configuration led to a more uniform field distribution than the wrap-around geometry. Specifically, sidewall conduction was seen to amplify the stray field from the counter electrode in comparison to the parallel electrode configuration. From this comparative analysis, we concluded that the field direction is vertical in the center of the counter electrode as in parallel-electrode configuration, while it eventually transitions to horizontal towards the edges, as in coplanar-electrode configurations, due to electrically active sidewalls.

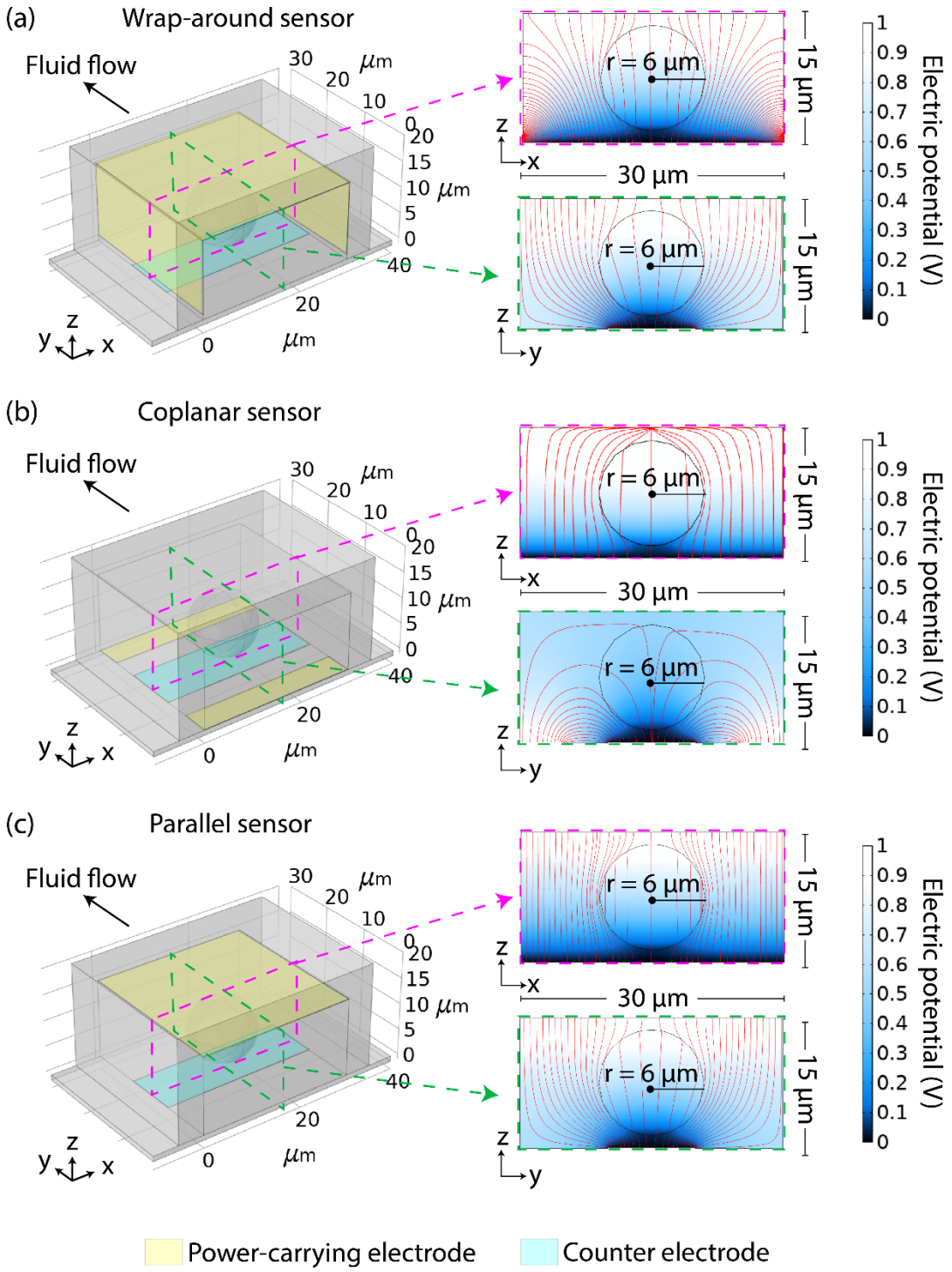

Figure 3. Simulation of E-field for different sensor geometries. Simulated 3D models (left) along with corresponding simulated electric field lines in two orthogonal cross-sections (right) are shown for three different scenarios: a microfluidic channel integrated with (a) the wrap-around sensor, (b) a sensor composed of a pair of coplanar electrodes placed on the channel floor and (c) a sensor made up of a surface electrode and a counter-facing parallel electrode on the channel ceiling.

Next, we investigated the effect of differences in field distributions on the sensitivity of the electrical sensor by calculating the changes in the electrical current between electrodes due to particle-induced electrical impedance variation (Figure 4). We first considered a biological cell interacting with electrode pairs at different vertical positions (10 μm – 55 μm) in a microfluidic channel that is 30 μm-wide and 65 μm-deep (Figure 4a). For both wrap-around and coplanar electrical sensors, the vertical position of the particle was found to affect the sensitivity, while the planar electrode sensor was agnostic to the vertical position resulting in a uniform change in the electrical current at different positions. The wrap-around was more sensitive than both coplanar and parallel electrode sensors for a cell 20 μm away from the surface. For higher elevations, the parallel-electrode sensor provided a higher sensitivity due to the higher concentration of the wrap-around sensor in the vicinity of the counter-electrode. Nevertheless, the wrap-around sensor was found to be ~3X more sensitive at all vertical positions compared to the sensor composed of coplanar electrodes.

We also investigated the response of our sensor for particles at different lateral positions across the width of the microfluidic channel using computer simulations (Materials and Methods) and compared its performance against the coplanar- and parallel-electrode sensors (Figure 4b). Even considering a relatively shallow (15 μm-deep and 30 μm-wide) channel, we found that a 12 μm-diameter cell, positioned at a vertical midpoint, led to greater (3-4X) changes in the electrical current for wrap-around and parallel-electrode sensors compared to the coplanar sensor across the channel width. While both parallel- and coplanar-electrode sensors remained agnostic to the lateral position of the particle, the wrap-around sensor's sensitivity was found to be increasing as the particle was positioned in the vicinity of the microfluidic channel sidewalls. This is expected the conductive sidewalls in our sensor lead to an extra current flow path between the counter electrode and the blanket electrode, and therefore, the same particle in different lateral positions would project varying magnitudes in impedance modulation. Specifically, we found that the particle can be detected with the highest sensitivity when it is closest to the sidewall. Taken together, the dependence of sensor response on lateral particle position has been found to be unique to the wrap-around sensor among the studied sensor geometries.

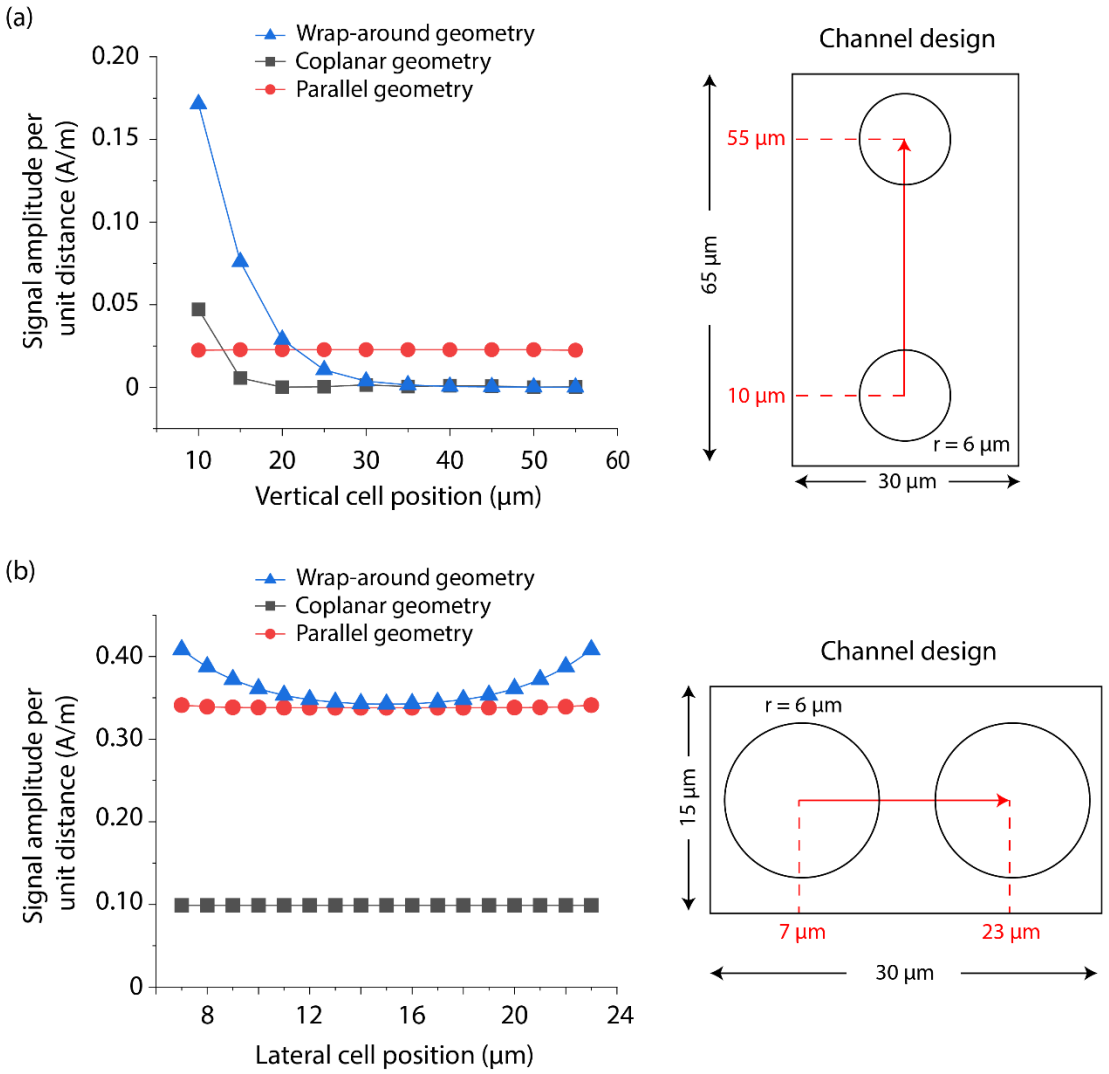

Figure 4. Computational analysis of particle position on sensor response. Plots show the simulated change in the electrical current flow between sensor electrodes as a function of (a) the vertical and (b) lateral cell positions in a microfluidic channel. The dimensions of the microfluidic channels employed for simulations in addition to the range of simulated vertical and lateral cell positions for the study are given in schematics. The diameter of the simulated cell was 12 µm.

3.4. Experimental Results

3.4.1. Sensor Characterization with Biological Samples

To experimentally characterize the wrap-around sensor, we created microfluidic devices integrated with those sensors using the previously described fabrication method. In these devices, both the blanket electrode and the counter electrode were made of 100 nm-thick gold film. The counter electrode was micromachined on a glass substrate as a 10 µm-wide finger cutting across the 30 µm-wide and 15 µm-high PDMS microfluidic channel (Figure 5a).

To test sensor functionality, we used our sensor to detect cultured human breast cancer cells (MDA-MB-231, Methods) suspended in 1X PBS, which was driven through the device at a flow rate of 100 µL/h (Materials and Methods).The sensor was electrically excited by

applying a 500 kHz signal with an amplitude of $0.1V_{pp}$ to the blanket electrode, and the current signal was collected from the counter electrode. Following amplification and conditioning of the signal, the data was sampled into a computer and analyzed using MATLAB (Materials and Methods). Analyzing 5 μL sample, we detected 4551 cells in 180 seconds, with a throughput of ~25 cells/second (Figure 5b). Our measured cell concentration of ~910 cells/μL was within ±3% of the independent measurement with a hematocytometer. Moreover, our calibrated measurements (Materials and Methods) of cell size resulted in an average diameter of ~13.8 μm, which closely matched with microscopy-based cell size measurements yielding an average cell diameter of ~13.52 μm.

Next, we directly compared the responses of the wrap-around sensor with a conventional sensor composed of micromachined coplanar electrodes by incorporating both sensors into the same microfluidic channel (Figure 5c). To fabricate this analytical device, we partially stencil-masked the PDMS layer with a Kapton tape and selectively deposited the gold film to form the blanket electrode of the wrap-around sensor (Materials and Methods). The surface electrodes were designed to be identical in dimensions for both sensors. To minimize electrical crosstalk between the two sensors, they were placed far (2 mm) apart, and also the coplanar electrode closer to the wrap-around sensor was ensured to equipotential with the blanket electrode by driving them with the same source. This arrangement of the two sensors within the same microfluidic channel allowed the same cell to sequentially interact with the sensors for a direct comparison between signals (Figure 5d).

Comparing signals from 3258 cells detected by both sensors, the wrap-around sensor provided a ~3.58X higher sensitivity on average compared to its coplanar counterpart, which agreed remarkably well with the simulation results presented earlier (Figure 5e). However, it should also be noted that the sensitivity enhancement for individual cells was observed to vary (Figure 5f), which was likely due to the differences between the response of each sensor to lateral and vertical positions of a particle in the microfluidic channel. In other words, even if a particle remains at the same vertical and lateral positions when interacting with both sensors, one would still expect different sensitivity enhancement factors at different locations, as seen from our numerical analysis on sensor response at different particle locations (Figure 4). Additionally, our wrap-around sensor differed from the coplanar sensor in terms of the pulse duration, leading to an average of ~28% shorter interaction times compared to the coplanar sensor for the identical cell population (Figure 5g). With the assumption that cells interacted with both sensors flowing at the same speed, the measured reduction in signal duration was attributed to confinement of the electric field in a smaller volume defined by a single 10 μm-wide surface electrode on the glass in the wrap-around sensor versus two 10 μm-wide surface electrodes separated by a 10 μm gap. The shorter interaction time of the wrap-around sensor could potentially be utilized to reduce coincident particles, a problem common with the analysis of suspensions with high particle density.

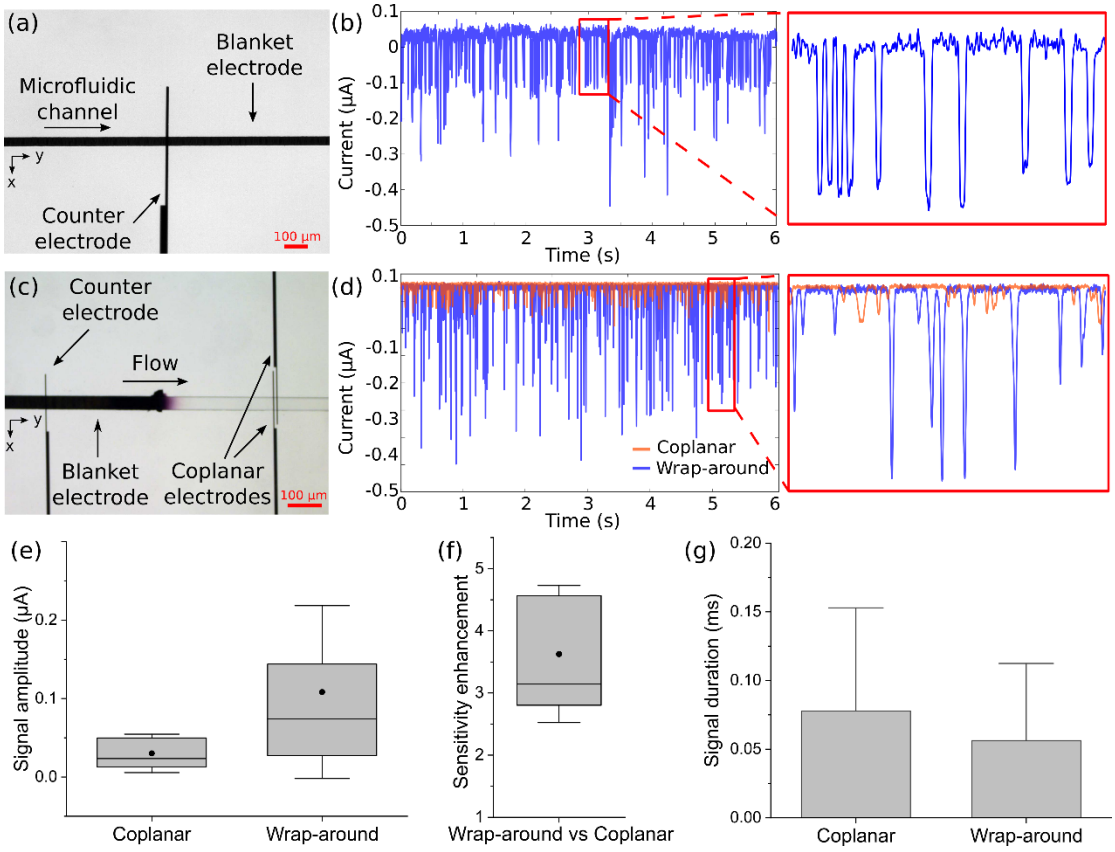

Figure 5. Sensor characterization with biological samples (a) A microscope image of a microfluidic channel integrated with a wrap-around sensor (b) Recorded wrap-around sensor signal showing electrical current modulation. (c) A microscope image of a microfluidic channel integrated with both a wrap-around sensor and a coplanar sensor for direct comparison of signals produced by the same cells. (d) Recoded electrical signals of the wrap-around sensor (blue) and the coplanar sensor (orange) from the sequential interaction of the sensors with the same cell population. (e) Measured signal amplitudes corresponding to the same 3258 cells detected by the wrap-around and coplanar sensors in the microfluidic device shown in (c). (f) Sensitivity enhancement provided by the wrap-around over an electrical sensor composed of coplanar electrodes. (g) Measured signal durations corresponding to the same 3258 cells detected by the wrap-around and coplanar sensors in the microfluidic device shown in (c). The box height denotes the mean, and the whisker denotes the standard deviation. For the bar graphs in (e) and (f), the dot denotes the mean; the line denotes the median; the box denotes the 25th and 75th percentiles, and the whisker denotes the standard deviation.

3.4.2. Testing of Multi-electrode Wrap-around Sensor Designs

We also attempted to construct wrap-around sensor geometries composed of more than a pair of electrodes. Electrical sensors in microfluidic devices are often built to include a third electrode, which helps eliminate common-mode signals in differential measurements and increases the sensitivity [36]. To create a differential wrap-around sensor, we coupled the blanket electrode to two different surface micromachined electrodes (Figure 6a). In this arrangement, the sensor was electrically through the blanket electrode with an AC voltage signal, and two surface electrodes were used to acquire two separate current signals, which

were subtracted with a differential amplifier to create a bipolar output signal (Figure 6b).

We functionally tested the differential wrap-around sensor fabricated within a microfluidic channel that is 30 μm-wide and 15-μm tall with a 5 μL of the prepared suspension of tumor cells. Detecting 4408 cells at a throughput of ~24.5 cells/second, the sensor's estimated sample concentration of 882 cells/μL was within <6% of the cell concentration of the prepared suspension (938 cells/μL) independently measured with a hemocytometer.

Next, we investigated the scaling of the wrap-around sensor geometry to create electrical sensor networks composed of complex electrode patterns. Specifically, we attempted to create coded impedance sensors composed of unique micromachined electrode patterns to generate distinct signal outputs for creating sensor networks. Using the mathematically orthogonal [37] or randomly generated codes [56], the signals from multiple sensors can be acquired from a single output and reliably distinguished from each other. Coded sensor networks have been realized using coplanar electrodes [35, 37] and were demonstrated to create flow cytometers [19, 57, 58], electronic antibody microarrays [20, 59] and autonomous microfluidic systems [57, 60]. On the other hand, scaling these sensor networks, when built using coplanar electrodes, required excessively long electrode traces, which lowered sensitivity due to high electrical resistance [36]. Here, we utilized a 7-bit Gold codes [61] that were generated as described by Liu et al. [37] as spreading sequences to multiplex the electrical sensors. We replaced the coplanar reference electrode that was conventionally placed to meander in between the two other coplanar electrodes with the blanket electrode (Figure 6c). By moving the reference electrode onto the microfluidic channel walls, the wrap-around sensor layout required only two coplanar electrodes to be routed on the surface, effectively eliminating the routing constraints and inefficiencies associated with the placement of the third coplanar electrode.

To test the responses of coded wrap-around sensors to flowing particles, we processed tumor cell suspension in a microfluidic device integrated with a network of four sensors. The whole sensor network was excited from the blanket electrode, and the current signals acquired from the two coplanar electrodes were subtracted from each other as the cells were driven through the microfluidic channels at a constant flow speed (100 μL/h). Each wrap-around sensor in the network was specifically designed to produce 7-bit digital codes ("0110101", "1111110", "0100010" and "0001100") orthogonal to each other so that they can be differentiated from each other through correlation. Analysis of the output signal from the device clearly showed four different code signals with individual bits in each digital code clearly recognizable (Figure 6d). Taken together, these results demonstrated the feasibility of constructing networks of coded wrap-around sensors for multiplexed detection of suspended particles in microfluidic devices.

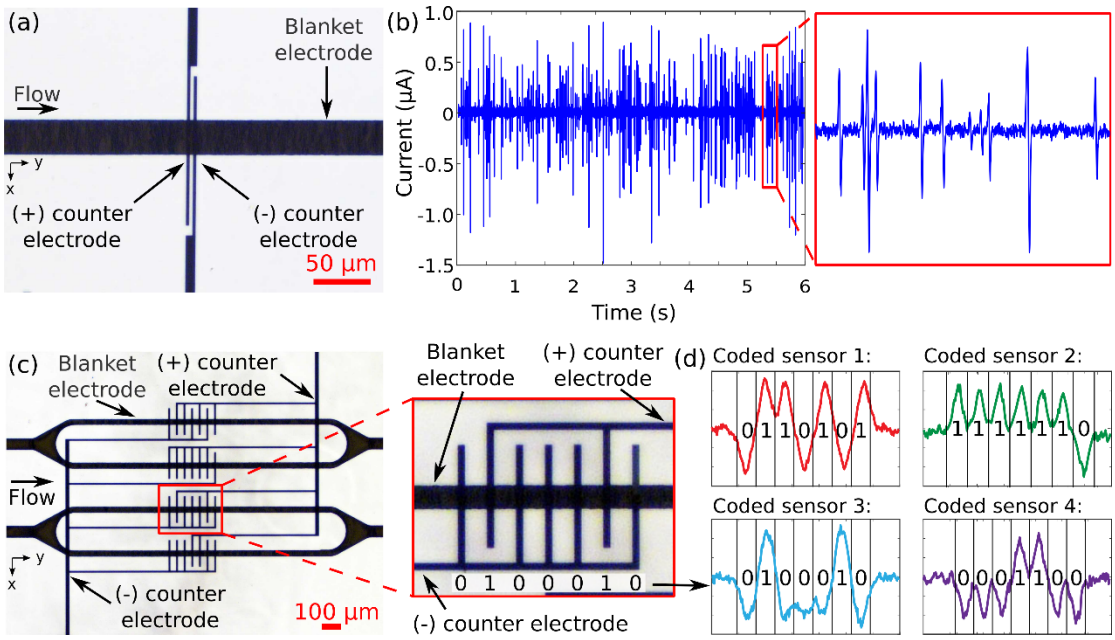

Figure 6. Testing of multi-electrode wrap-around sensor designs. (a) A microscope image of a differential wrap-around sensors composed of a blanket electrode and two counter electrodes on the floor of the microfluidic channel. (b) Recorded electrical signal from the differential wrap-around sensor. (c) A microscope image of a microfluidic device integrated with a network of four coded wrap-around sensors. The close-up of one of the coded wrap-around sensors shows the code generating electrode fingers and the corresponding digital code that the sensor produced. (d) Recorded signals from individual code-multiplexed wrap-around sensors in the network. The sensor signals could be seen to follow the underlying electrode pattern for each coded wrap-around sensor and clearly differ from each other.

4. DISCUSSION

In this work, we introduced an electrical sensor that wraps around microfluidic channels for electronic detection, characterization and tracking of electrolyte-suspended particles. Our wrap-around sensor distributes the electric field more uniformly throughout a microfluidic channel cross-section than conventionally employed impedance sensors constructed with coplanar electrodes and is more sensitive for a given aperture size. Therefore, our work offers the potential to increase the utility of electrical sensing particularly for the detection of smaller particles such as bacteria or viruses, which can directly benefit from the enhanced sensitivity offered by our sensor. Compared to the existing microfabrication methods for 3D electrical sensors in microfluidics, such as etching [43] or multi-stage photolithography [46], our process offers a conformal sensor structure in relatively simple removal step using conventional adhesive tapes. While etching methods [43] and atomic level modifications [42] would face a trade-off in throughput and time for thickness control, our throughput is indifferent to the thickness of the metal layer as the excess material would be removed in bulk in a single step.

Importantly, we developed a fabrication process that allowed our wrap-around electrical sensors to be readily integrated into microfluidic devices created using soft lithography. Considering that the electrical sensors based on coplanar electrodes have long been the design

of choice, effectively trading higher sensitivity and more robust measurements for a simple and self-aligned fabrication process, the practical fabrication method introduced in this work alleviates this long-standing trade-off faced when creating 3D electrical sensors in PDMS-based microfluidic devices. Moreover, our fabrication method can potentially be modified to employ a non-conformal metal deposition technique such as electron beam deposition [62] and utilize shadows in deposition to exclusively deposit the metal film on the microfluidic channel ceiling (i.e., with no sidewall coating) to create a sensor with counter-facing parallel electrodes. Likewise, our process can also be tailored to selectively deposit electrodes only onto a subset of the inner walls of a microfluidic channel via deposition at an angle to realize a variety of 3D electrode configurations, that otherwise would not be possible to manufacture using conventional fabrication techniques.

We have also shown that wrap-around sensors differ in their response to particles in microfluidic channels than sensors built using coplanar electrodes or counter-facing parallel electrodes. Specifically, the sensitivity of the wrap-around sensor to the lateral position of particles in a microfluidic channel can be minimized by tuning microfluidic channel dimensions to spatially confine a cell. This would not only reduce errors in applications focusing on cell size measurements but also improve the sensitivity. On the other hand, the lateral position dependency can potentially provide additional spatial information when paired with a reference sensor that is insensitive to lateral position (e.g., conventional lateral-position-insensitive electrode configurations). In a differential and calibrated measurement, the effects of other dependencies, i.e., size and vertical position, can be negated based on data from position-insensitive electrodes and the lateral position can be extracted from our signal as the only remaining variable. Given downstream lateral positions of sorted particles in a microfluidic channel can be linked to the particle properties [19, 57, 58], spatial sensitivity of our wrap-around sensors can potentially be utilized as an electrical readout for particle characterization. Beyond sensing applications, the non-uniform electric field can be utilized for dielectrophoretic manipulation of particles in contrast with parallel-electrode sensors with uniform field distribution.

Inclusion of the wide blanket electrode within the wrap-around sensor did not produce additional noise compared to other electrode geometries in our experiments. On the contrary, the signal-to-noise ratio improved for detection of cells due sensitivity enhancement. It is also expected that the blanket electrode will improve signal- signal-to-noise ratio particularly for electrode designs with excessively long narrow electrode traces. As previously demonstrated, the length of a micromachined electrode trace indeed plays a role in the signal quality [36]. In our experiments, we demonstrated a throughput of 25 cells per second; however, this value does not represent a limit on the achievable measurement throughput using our sensor. In fact, impedance-based sensors in lab-on-a-chip devices were shown to achieve a throughput in the order of 1000 of cells per second [56]. On the other hand, the optical opacity of the blanket electrode covering microfluidic channels can be considered as a limitation for applications involving microscopy. These limitations can potentially be circumvented either by creating imaging slits by stencil masking, imaging the device from the counter electrode side in an epi-illumination setup or by manufacturing the blanket electrode out of a transparent material such indium tin oxide.

Finally, the availability of a blanket electrode running along the microfluidic channels effectively carries the electric field to wherever the fluid is carried, which significantly simplifies the creation of electrical sensors at desired locations, helps integrate a large number of sensors into a microfluidic device without increasing the device complexity. With the proposed approach in this work, in any location where a surface electrode meets with the metal-coated microfluidic channel, an electrical sensor is created. In addition, because the sensing zone is defined by the overlap between the blanket and the surface electrode, a precise alignment is not required to create a microscale electrical sensor. The downside of this design flexibility is the unintended creation of sensors whenever a surface electrode is needed to be routed across a microfluidic channel. This problem can potentially be addressed by stencil-masking of the metal deposition on the microfluidic layer to create "blind-spots", where channel crossings can be made without creating active sensing zones.

5. CONCLUSIONS

We reported a 3D electrical sensor that relies on conductive inner walls of a microfluidic channel for the detection of suspended particles with higher sensitivity than conventional electrical sensors consisting of coplanar electrode pairs. Our sensor can readily be integrated into polymer-based microfluidic devices through a fabrication process that is inherently compatible with the soft lithography process, and the simplicity of the developed fabrication process further enhances the impact of our work offering a practical solution to implement 3D wrap-around sensors in a variety of quantitative microfluidic assays. Besides higher sensitivity and scalability, wrap-around sensors differ from conventional electrode layouts in their response to particle position and its properties, and therefore, offer exciting opportunities for extracting complementary information on samples.

AUTHOR CONTRIBUTIONS

O.C., R.L. and A.F.S. designed the research. R.L., A.K.M.A., N.A. performed the microfabrication. R.L. conducted the characterization experiments. O.C. and R.L. did the computational analysis. O.C., R.L., N.A. and A.F.S. wrote the manuscript.

CONFLICT OF INTEREST

The authors declare no competing interests.

ACKNOWLEDGEMENTS

The work was sponsored by National Science Foundation (NSF) via grants ECCS 1610995 and ECCS 1752170, and by Arnold and Mabel Beckman Foundation via Beckman Young Investigator Award to A.F.S. The authors would like to thank Mr. Hang Chen and other cleanroom staff at Institute for Electronics and Nanotechnology for their suggestions.

REFERENCES

[1] B. Ronain Smith, M. Ruegsegger, P.A. Barnes, M. Ferrari, S.C. Lee, Nanodevices in biomedical applications, BioMEMS and Biomedical Nanotechnology, Springer2006, pp. 363-98.

[2] X. Zhang, Gold Nanoparticles: Recent Advances in the Biomedical Applications, Cell Biochemistry and Biophysics, 72(2015) 771-5.

[3] S. Gupta, K. Ramesh, S. Ahmed, V. Kakkar, Lab-on-chip technology: A review on design trends and future scope in biomedical applications, Int J Bio-Sci Bio-Technol, 8(2016) 311-22.
[4] W.-T. Liu, Nanoparticles and their biological and environmental applications, Journal of Bioscience and Bioengineering, 102(2006) 1-7.
[5] M. Yew, Y. Ren, K.S. Koh, C. Sun, C. Snape, A Review of State-of-the-Art Microfluidic Technologies for Environmental Applications: Detection and Remediation, Global Challenges, 3(2019) 1800060.
[6] Y. Shen, Q. Fang, B. Chen, Environmental Applications of Three-Dimensional Graphene-Based Macrostructures: Adsorption, Transformation, and Detection, Environmental Science & Technology, 49(2015) 67-84.
[7] J. Gross-Rother, M. Blech, E. Preis, U. Bakowsky, P. Garidel, Particle Detection and Characterization for Biopharmaceutical Applications: Current Principles of Established and Alternative Techniques, Pharmaceutics, 12(2020) 1112.
[8] J. Comas-Riu, N. Rius, Flow cytometry applications in the food industry, Journal of Industrial Microbiology and Biotechnology, 36(2009) 999-1011.
[9] W.H. Coulter, High speed automatic blood cell counter and cell size analyzer, Proceedings of the National Electronics Conference1956, p. 1034.
[10] J. Hurley, Sizing Particles with a Coulter Counter, Biophysical Journal, 10(1970) 74-9.
[11] C. Honrado, P. Bisegna, N.S. Swami, F. Caselli, Single-cell microfluidic impedance cytometry: from raw signals to cell phenotypes using data analytics, Lab on a Chip, 21(2021) 22-54.
[12] M. Shaker, L. Colella, F. Caselli, P. Bisegna, P. Renaud, An impedance-based flow microcytometer for single cell morphology discrimination, Lab on a Chip, 14(2014) 2548-55.
[13] J. Stetefeld, S.A. McKenna, T.R. Patel, Dynamic light scattering: a practical guide and applications in biomedical sciences, Biophysical Reviews, 8(2016) 409-27.
[14] M.N. Rhyner, The Coulter Principle for Analysis of Subvisible Particles in Protein Formulations, The AAPS Journal, 13(2011) 54-8.
[15] G. Luka, A. Ahmadi, H. Najjaran, E. Alocilja, M. DeRosa, K. Wolthers, et al., Microfluidics Integrated Biosensors: A Leading Technology towards Lab-on-a-Chip and Sensing Applications, Sensors, 15(2015) 30011-31.
[16] R. Rodriguez-Trujillo, M.A. Ajine, A. Orzan, M.D. Mar, F. Larsen, C.H. Clausen, et al., Label-free protein detection using a microfluidic Coulter-counter device, Sensors and Actuators B: Chemical, 190(2014) 922-7.
[17] J. Berger, E. Valera, A. Jankelow, C. Garcia, M. Akhand, J. Heredia, et al., Simultaneous electrical detection of IL-6 and PCT using a microfluidic biochip platform, Biomedical Microdevices, 22(2020) 36.
[18] A.V. Jagtiani, J. Zhe, J. Hu, J. Carletta, Detection and counting of micro-scale particles and pollen using a multi-aperture Coulter counter, Measurement Science and Technology, 17(2006) 1706.
[19] O. Civelekoglu, R. Liu, C.F. Usanmaz, C.-H. Chu, M. Boya, T. Ozkaya-Ahmadov, et al., Electronic measurement of cell antigen expression in whole blood, Lab on a Chip, (2022).
[20] R. Liu, C.-H. Chu, N. Wang, T. Ozkaya-Ahmadov, O. Civelekoglu, D. Lee, et al., Combinatorial Immunophenotyping of Cell Populations with an Electronic Antibody Microarray, Small, 15(2019) 1904732.

[21] A. De Ninno, R. Reale, A. Giovinazzo, F.R. Bertani, L. Businaro, P. Bisegna, et al., High-throughput label-free characterization of viable, necrotic and apoptotic human lymphoma cells in a coplanar-electrode microfluidic impedance chip, Biosensors and Bioelectronics, 150(2020) 111887.
[22] J. Yan, C. Wang, Y. Fu, J. Guo, J. Guo, 3D printed microfluidic Coulter counter for blood cell analysis, Analyst, (2022).
[23] N. Khodaparastasgarabad, A. Mohebbi, C. Falamaki, A novel microfluidic high-throughput resistive pulse sensing device for cells analysis, Microsystem Technologies, 25(2019) 3643-53.
[24] A.C. Stelson, M. Liu, C.A.E. Little, C.J. Long, N.D. Orloff, N. Stephanopoulos, et al., Label-free detection of conformational changes in switchable DNA nanostructures with microwave microfluidics, Nature Communications, 10(2019) 1174.
[25] C. Allen, J.F. Loo, S. Yu, S. Kong, T.-F. Chan, Monitoring bacterial growth using tunable resistive pulse sensing with a pore-based technique, Applied microbiology and biotechnology, 98(2014) 855-62.
[26] Y. Yang, K. Gupta, K.L. Ekinci, All-electrical monitoring of bacterial antibiotic susceptibility in a microfluidic device, Proceedings of the National Academy of Sciences, 117(2020) 10639-44.
[27] E. Bogomolny, J. Hong, C. Blenkiron, D. Simonov, P. Dauros, S. Swift, et al., Analysis of bacteria-derived outer membrane vesicles using tunable resistive pulse sensing: SPIE; 2015.
[28] R.E. Lane, D. Korbie, W. Anderson, R. Vaidyanathan, M. Trau, Analysis of exosome purification methods using a model liposome system and tunable-resistive pulse sensing, Scientific Reports, 5(2015) 7639.
[29] K.C. Cheung, M. Di Berardino, G. Schade‐Kampmann, M. Hebeisen, A. Pierzchalski, J. Bocsi, et al., Microfluidic impedance‐based flow cytometry, Cytometry Part A, 77(2010) 648-66.
[30] T. Vaclavek, J. Prikryl, F. Foret, Resistive pulse sensing as particle counting and sizing method in microfluidic systems: Designs and applications review, Journal of Separation Science, 42(2019) 445-57.
[31] D. Qin, Y. Xia, G.M. Whitesides, Soft lithography for micro-and nanoscale patterning, Nature protocols, 5(2010) 491.
[32] V. Errico, A.D. Ninno, F.R. Bertani, L. Businaro, P. Bisegna, F. Caselli, Mitigating positional dependence in coplanar electrode Coulter-type microfluidic devices, Sensors and Actuators B: Chemical, 247(2017) 580-6.
[33] C.H. Clausen, G.E. Skands, C.V. Bertelsen, W.E. Svendsen, Coplanar electrode layout optimized for increased sensitivity for electrical impedance spectroscopy, Micromachines, 6(2015) 110-20.
[34] J. Hong, D.S. Yoon, S.K. Kim, T.S. Kim, S. Kim, E.Y. Pak, et al., AC frequency characteristics of coplanar impedance sensors as design parameters, Lab on a Chip, 5(2005) 270-9.
[35] R. Liu, W. Waheed, N. Wang, O. Civelekoglu, M. Boya, C.-H. Chu, et al., Design and modeling of electrode networks for code-division multiplexed resistive pulse sensing in microfluidic devices, Lab on a Chip, 17(2017) 2650-66.
[36] R. Liu, N. Wang, N. Asmare, A.F. Sarioglu, Scaling code-multiplexed electrode networks

for distributed Coulter detection in microfluidics, Biosensors and Bioelectronics, 120(2018) 30-9.
[37] R. Liu, N. Wang, F. Kamili, A.F. Sarioglu, Microfluidic CODES: a scalable multiplexed electronic sensor for orthogonal detection of particles in microfluidic channels, Lab on a Chip, 16(2016) 1350-7.
[38] T. Sun, N.G. Green, S. Gawad, H. Morgan, Analytical electric field and sensitivity analysis for two microfluidic impedance cytometer designs, IET nanobiotechnology, 1(2007) 69-79.
[39] S. Gawad, L. Schild, P. Renaud, Micromachined impedance spectroscopy flow cytometer for cell analysis and particle sizing, Lab on a Chip, 1(2001) 76-82.
[40] G. Mernier, E. Duqi, P. Renaud, Characterization of a novel impedance cytometer design and its integration with lateral focusing by dielectrophoresis, Lab on a Chip, 12(2012) 4344-9.
[41] F. Caselli, P. Bisegna, F. Maceri, EIT-Inspired Microfluidic Cytometer for Single-Cell Dielectric Spectroscopy, Journal of Microelectromechanical Systems, 19(2010) 1029-40.
[42] B. Atmaja, J. Frommer, J.C. Scott, Atomically Flat Gold on Elastomeric Substrate, Langmuir, 22(2006) 4734-40.
[43] K.W. Meacham, R.J. Giuly, L. Guo, S. Hochman, S.P. DeWeerth, A lithographically-patterned, elastic multi-electrode array for surface stimulation of the spinal cord, Biomedical Microdevices, 10(2008) 259-69.
[44] I. Byun, A.W. Coleman, B. Kim, Transfer of thin Au films to polydimethylsiloxane (PDMS) with reliable bonding using (3-mercaptopropyl) trimethoxysilane (MPTMS) as a molecular adhesive, Journal of Micromechanics and Microengineering, 23(2013) 085016.
[45] J. Lee, M. Wipf, L. Mu, C. Adams, J. Hannant, M.A. Reed, Metal-coated microfluidic channels: An approach to eliminate streaming potential effects in nano biosensors, Biosensors and Bioelectronics, 87(2017) 447-52.
[46] N. Mamun, P. Dutta, Patterning of platinum microelectrodes in polymeric microfluidic chips, Journal of Micro/Nanolithography, MEMS, and MOEMS, 5(2006) 039701.
[47] K. Cheung, S. Gawad, P. Renaud, Impedance spectroscopy flow cytometry: On-chip label-free cell differentiation, Cytometry Part A, 65A(2005) 124-32.
[48] D. Spencer, F. Caselli, P. Bisegna, H. Morgan, High accuracy particle analysis using sheathless microfluidic impedance cytometry, Lab on a Chip, 16(2016) 2467-73.
[49] D.K. Wood, M.V. Requa, A.N. Cleland, Microfabricated high-throughput electronic particle detector, Review of Scientific Instruments, 78(2007) 104301.
[50] D. Spencer, H. Morgan, Positional dependence of particles in microfludic impedance cytometry, Lab on a Chip, 11(2011) 1234-9.
[51] N. Haandbæk, O. With, S.C. Bürgel, F. Heer, A. Hierlemann, Resonance-enhanced microfluidic impedance cytometer for detection of single bacteria, Lab on a Chip, 14(2014) 3313-24.
[52] T.L. Edwards, J.C. Harper, R. Polsky, D.M. Lopez, D.R. Wheeler, A.C. Allen, et al., A parallel microfluidic channel fixture fabricated using laser ablated plastic laminates for electrochemical and chemiluminescent biodetection of DNA, Biomicrofluidics, 5(2011) 044115.
[53] L. Wu, L.-Y.L. Yung, K.-M. Lim, Dielectrophoretic capture voltage spectrum for measurement of dielectric properties and separation of cancer cells, Biomicrofluidics, 6(2012) 014113.

[54] M. Jurczak, N. Collaert, A. Veloso, T. Hoffmann, S. Biesemans, Review of FINFET technology, 2009 IEEE International SOI Conference2009, pp. 1-4.
[55] E.J. Nowak, I. Aller, T. Ludwig, K. Kim, R.V. Joshi, C. Ching-Te, et al., Turning silicon on its edge [double gate CMOS/FinFET technology], IEEE Circuits and Devices Magazine, 20(2004) 20-31.
[56] N. Wang, R. Liu, N. Asmare, C.-H. Chu, A.F. Sarioglu, Processing code-multiplexed Coulter signals via deep convolutional neural networks, Lab on a Chip, 19(2019) 3292-304.
[57] O. Civelekoglu, N. Wang, A.K.M. Arifuzzman, M. Boya, A.F. Sarioglu, Automated lightless cytometry on a microchip with adaptive immunomagnetic manipulation, Biosensors and Bioelectronics, 203(2022) 114014.
[58] O. Civelekoglu, N. Wang, M. Boya, T. Ozkaya-Ahmadov, R. Liu, A.F. Sarioglu, Electronic profiling of membrane antigen expression via immunomagnetic cell manipulation, Lab on a Chip, 19(2019) 2444-55.
[59] R. Liu, A.K.M. Arifuzzman, N. Wang, O. Civelekoglu, A.F. Sarioglu, Electronic Immunoaffinity Assay for Differential Leukocyte Counts, Journal of Microelectromechanical Systems, 29(2020) 942-7.
[60] N. Wang, R. Liu, N. Asmare, C.-H. Chu, O. Civelekoglu, A.F. Sarioglu, Closed-loop feedback control of microfluidic cell manipulation via deep-learning integrated sensor networks, Lab on a Chip, 21(2021) 1916-28.
[61] R. Gold, Optimal binary sequences for spread spectrum multiplexing (corresp.), IEEE Transactions on information theory, 13(1967) 619-21.
[62] S.I. Shah, G.H. Jaffari, E. Yassitepe, B. Ali, Chapter 4 - Evaporation: Processes, Bulk Microstructures, and Mechanical Properties, in: P.M. Martin (Ed.) Handbook of Deposition Technologies for Films and Coatings (Third Edition), William Andrew Publishing, Boston, 2010, pp. 135-252.

Supplementary Information

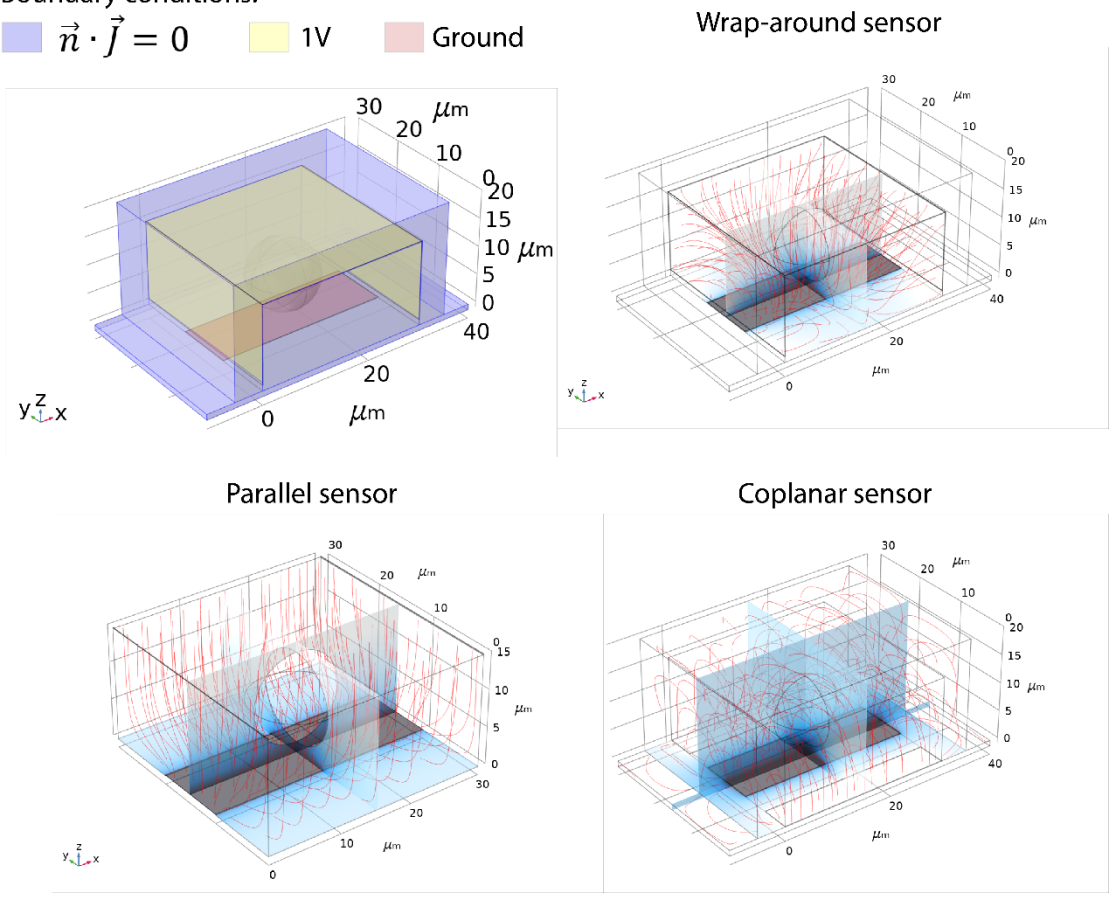

Supplementary Figure 1: 3D simulations of electric field lines for the sensor geometries illustrated in Figure 3.